Solar Phys (2011) 274:99–117
DOI 10.1007/s11207-011-9755-0

The State of Self-organized Criticality of the Sun During the Last Three Solar Cycles. I. Observations

Markus J. Aschwanden

Received: 24 June 2010 / Accepted: 14 March 2011 / Published online: 21 April 2011

Abstract We analyze the occurrence-frequency distributions of peak fluxes $[P]$, total fluxes $[E]$, and durations $[T]$ of solar flares over the last three solar cycles (during 1980 – 2010) from SMM/HXRBS, CGRO/BATSE, and RHESSI hard X-ray data. From the synthesized data we find powerlaw slopes with mean values of $\alpha_P = 1.73 \pm 0.07$ for the peak flux, $\alpha_E = 1.62 \pm 0.12$ for the total flux, and $\alpha_T = 1.99 \pm 0.35$ for flare durations. We find a tendency of an anti-correlation of the powerlaw slope of peak fluxes with the flare rate or sunspot number as a function of the solar cycle. The occurrence powerlaw slope is always steeper by $\Delta\alpha \approx 0.1$ during a solar-cycle minimum compared with the previous solar-cycle maximum, but the relative amplitude varies for each cycle or instrument. Since each solar cycle has been observed with a different instrument, part of the variation could be attributed to instrumental characteristics and different event selection criteria used in generating the event catalogs. The relatively flatter powerlaw slopes during solar maxima could indicate more energetic flares with harder electron-energy spectra, probably due to a higher magnetic complexity of the solar corona. This would imply a non-stationarity (or solar-cycle dependence) of the coronal state of self-organized criticality.

Keywords Sun: hard X-rays · Sun: flares · Solar cycle

1. Introduction

In the observational part of this study (Paper I) we focus on the statistics of solar-flare hard X-ray fluxes during the course of the last three solar cycles, while theoretical modeling is referred to Paper II. Solar flares are catastrophic events in the solar corona, most likely caused by a magnetic instability that triggers a magnetic reconnection process, producing emission

The Sun–Earth Connection near Solar Minimum
Guest Editors: M.M. Bisi, B. Emery, and B.J. Thompson

M.J. Aschwanden (✉)
Solar and Astrophysics Laboratory, Dept. ADBS, Lockheed Martin Advanced Technology Center, Bldg.252, 3251 Hanover St., Palo Alto, CA 94304, USA
e-mail: aschwanden@lmsal.com

in almost all wavelengths. Since the emission mechanisms are all different in each wavelength, such as nonthermal bremsstrahlung (in hard X-rays), thermal bremsstrahlung and free-bound or recombination radiation (in soft X-rays and EUV), gyrosynchrotron emission (in microwaves), plasma emission (in metric and decimetric waves), *etc*., estimates of the energy contained in each flare event strongly depend on the emission mechanism, and thus on the wavelength. In this study we concentrate on the hard X-ray wavelength. Hard X-ray emission in solar flares mostly results from thick-target bremsstrahlung of nonthermal electrons accelerated in the corona that precipitate into the dense chromosphere. Thus, the hard X-ray flux is the most direct measure of the energy-release rate, and thus is expected to characterize the energy of flare events in a most uncontaminated way, while emission in other wavelengths exhibits a more convolved evolution of secondary emission processes. The main observables that are available for flare statistics in hard X-rays are the peak flux $[P]$, the total flux or fluence $[E]$ (defined as the time-integrated flux over the entire event), and the total time duration $[T]$ of the event. In this study, we present a comprehensive compilation of occurrence-frequency distributions of these observables obtained in hard X-rays, and investigate whether their behavior is different during solar-cycle minima, including the current anomalous solar minimum.

2. Statistics of Solar Flares in Hard X-rays

In this section we describe observed occurrence-frequency distributions of solar-flare hard X-ray parameters (in chronological order), discuss the properties of the datasets (hard X-ray energies, observational epochs, instruments), compile the results in Table 1 (powerlaw slopes of fluxes, fluences, durations, number of events, instruments, and references), and derive synthesized distributions that serve as reference values of the average solar-flare activity. In Section 4 we investigate whether deviations from these reference values can be found during the solar cycle.

One of the earliest reports of a frequency distribution of solar hard X-ray flare fluxes was made by Datlowe, Elcan, and Hudson (1974), who published a frequency distribution of 123 flare events detected in the 20 – 30 keV energy range above a threshold of $\gtrsim 0.1$ photons $\mathrm{cm}^{-2}\,\mathrm{s}^{-1}\,\mathrm{keV}^{-1}$ with the OSO-7 spacecraft during the period of 10 October 1971 – 6 June 1972, finding a powerlaw slope of $\beta_P \approx 0.8$ for the cumulative frequency distribution. For compatibility we list only powerlaw slopes $[\alpha]$ of differential frequency distributions in Table 1, and use the conversion $\alpha = \beta + 1$ when needed. We list also the number of events, which is a good indicator of the statistical uncertainty of the powerlaw slope fits (Figure 6).

A sample of 25 microflares of smaller size were detected at 20 keV with a balloon-borne instrumentation of the University of California Berkeley (UCB) during 141 minutes of observations on 27 June 1980, yielding a powerlaw distribution with a slope of $\beta \approx 1$ (Lin *et al.*, 1984).

Many more events were observed with the *Hard X-Ray Burst Spectrometer* (HXRBS) onboard the *Solar Maximum Mission* (SMM) spacecraft, which recorded 6775 flare events during the 1980 – 1985 period, exhibiting a powerlaw distribution of peak count rates with a slope of $\alpha_P = 1.8$, extending over four orders of magnitude (Dennis, 1985).

A subsequent mission with hard X-ray detector capabilities was the *Compton Gamma Ray Observatory* (CGRO). Although it was designed to detect γ-rays from astrophysical objects, it also detected solar flares systematically during the period of 1991 – 2000. Using the *Burst And Source Transient Experiment* (BATSE), statistics of flares with energies > 25 keV were sampled and more detailed powerlaw distributions of peak fluxes were reported with values of $\alpha_P = 1.61 \pm 0.03$ (Schwartz *et al.*, 1992), $\alpha_P = 1.75 \pm 0.02$ (Biesecker,

Table 1 Frequency distributions measured from solar flares in hard X-rays and γ-rays. References: [1] Datlowe, Elcan, and Hudson (1974); [2] Lin *et al.* (1984); [3] Dennis (1985); [4] Schwartz *et al.* (1992); [5] Crosby, Aschwanden, and Dennis (1993); [6] Biesecker, Ryan, and Fishman (1993); [7] Biesecker, Ryan, and Fishman (1994); [8] Crosby (1996); [9] Lu *et al.* (1993); [10] Lee, Petrosian, and McTiernan (1993); [11] Bromund, McTiernan, and Kane (1995); [12] Perez Enriquez and Miroshnichenko (1999); [13] Su, Gan, and Li (2006); [14] Christe *et al.* (2008); [15] Lin, Feffer, and Schwartz (2001); [16] Tranquille, Hurley, and Hudson (2009).

Powerlaw slope of peak flux [α_P]	Powerlaw slope of fluence [α_E]	Powerlaw slope of durations [α_T]	Number of events [n]	Instrument and threshold energy	Reference
1.8			123	OSO-7 (>20 keV)	1
2.0			25	UCB (>20 keV)	2
1.8			6775	HXRBS (>20 keV)	3
1.73±0.01			12 500	HXRBS (>25 keV)	4
1.73±0.01	1.53±0.02	2.17±0.05	7045	HXRBS (>25 keV)	5
1.71±0.04	1.51±0.04	1.95±0.09	1008	HXRBS (>25 keV)	5
1.68±0.07	1.48±0.02	2.22±0.13	545	HXRBS (>25 keV)	5
1.67±0.03	1.53±0.02	1.99±0.06	3874	HXRBS (>25 keV)	5
1.61±0.03			1263	BATSE (>25 keV)	4
1.75±0.02			2156	BATSE (>25 keV)	6
1.79±0.04			1358	BATSE (>25 keV)	7
1.59±0.02		2.28±0.08	1546	WATCH (>10 keV)	8
1.86	1.51	1.88	4356	ISEE-3 (>25 keV)	9
1.75	1.62	2.73	4356	ISEE-3 (>25 keV)	10
1.86±0.01	1.74±0.04	2.40±0.04	3468	ISEE-3 (>25 keV)	11
1.80±0.01	1.39±0.01		110	PHEBUS (>100 keV)	12
1.80±0.02		2.2±1.4	2759	RHESSI (>12 keV)	13
1.58±0.02	1.7±0.1	2.2±0.2	4241	RHESSI (>12 keV)	14
1.6			243	BATSE (>8 keV)	15
1.61±0.04			59	ULYSSES (>25 keV)	16

Ryan, and Fishman, 1993), and $\alpha_P = 1.79 \pm 0.04$ (Biesecker, Ryan, and Fishman, 1994) for BATSE. Biesecker (1994) noticed slight differences of the powerlaw slope during low-activity ($\alpha_P = 1.71 \pm 0.04$) and high-activity periods ($\alpha_P = 1.68 \pm 0.02$), with the powerlaw slope being usually flatter for high-activity periods.

A systematic study of flares observed with HXRBS over the entire mission duration of 1980 – 1989 was conducted by Crosby, Aschwanden, and Dennis (1993), measuring peak count rates [$P_{\rm cts}$: cts s^{-1}], converted into photon fluxes [$P_{\rm ph}$: photons cm^{-2} s^{-1} keV^{-1}] at energies > 25 keV, peak HXR spectrum-integrated fluxes [$P_{\rm X}$: photons cm^{-1} s^{-1}], peak electron fluxes [$P_{\rm e}$: ergs s^{-1}], flare durations T, and time-integrated total energies in electrons [$E_{\rm e}$: ergs], for four different time intervals of the solar cycle. In Table 1 we list the values for the time ranges of 1980 – 1982 (7045 events; solar maximum phase), 1983 – 1984 (1008 events), 1985 – 1987 (545 events; solar minimum phase), and 1988 – 1989 (3874 events). The values of the powerlaw slopes change by $\lesssim 2\%$ during different periods of the solar cycle.

From the *Wide Angle Telescope for Cosmic Hard X-Rays* (WATCH) onboard the Russian satellite GRANAT, a sample of 1546 flare events was observed at energies of

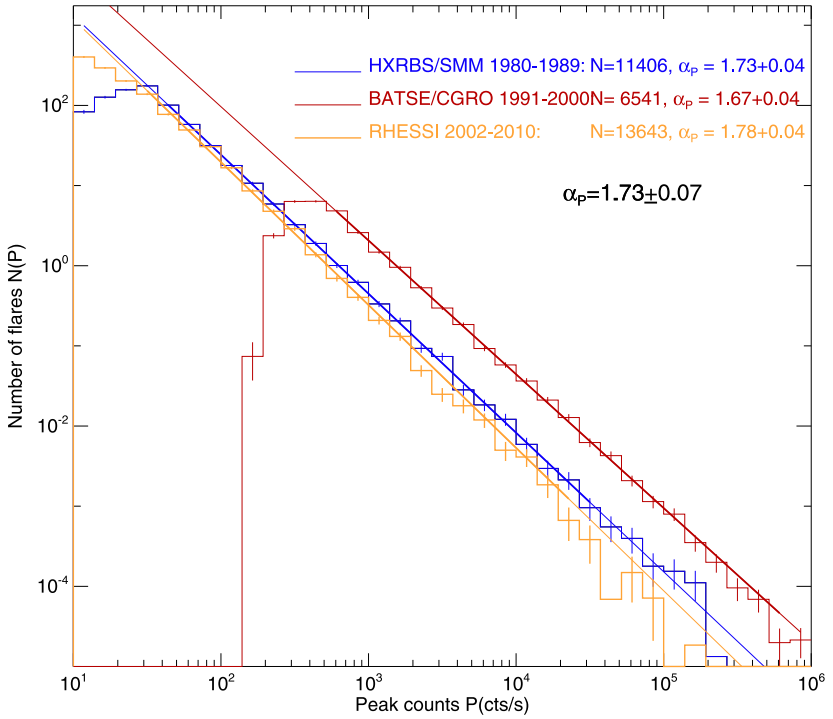

Figure 1 Occurrence-frequency distributions of hard X-ray peak count rates [$P_{\rm cts}$: cts s^{-1}] observed with SMM/HXRBS (1980 – 1989), BATSE (1991 – 2000), and RHESSI (2002 – 2010), with powerlaw fits. An average preflare background of 40 [cts s^{-1}] was subtracted from the HXRBS count rates. Note that CGRO/BATSE has larger detector areas, and thus records higher count rates.

10 – 30 keV during 1990 – 1992, yielding similar powerlaw slopes for peak count rates, $\alpha_P = 1.59 \pm 0.02$, and flare durations $\alpha_T = 2.28 \pm 0.08$ as reported before (Crosby, 1996; Crosby *et al.*, 1998). However, it was noted that the frequency distribution of flare durations exhibits a gradual rollover for short flare durations, approaching a slope of $\alpha_T \approx 1$, so it cannot be fitted with a single powerlaw distribution over the entire range of flare durations. From the PHEBUS instrument on GRANAT, which is sensitive to γ-ray energies, Perez Enriquez and Miroshnichenko (1999) analyzed 110 high-energy solar flares observed in the energy range of 100 keV – 100 MeV and found the following powerlaw slopes: $\alpha_P = 1.80 \pm 0.01$ for (bremsstrahlung) hard X-ray fluxes at > 100 keV, $\alpha_P = 1.38 \pm 0.01$ for photon energies at 0.075 – 124 MeV, $\alpha_P = 1.39 \pm 0.01$ for bremsstrahlung at 300 – 850 keV, $\alpha_E = 1.50 \pm 0.03$ for the 511 keV annihilation line fluence, $\alpha_E = 1.39 \pm 0.02$ for the 2.223 MeV neutron-line fluence, and $\alpha_E = 1.31 \pm 0.01$ for the 1 – 10 MeV γ-ray line fluence. The flatter powerlaw slopes of the occurrence-frequency distributions at higher energies could possibly be explained by flatter spectra (Section 3.1).

Using data from $a > 25$ keV hard X-ray detector onboard the ISEE-3/ICE spacecraft from 24 August 1978 until 11 July 1986, Lu *et al.* (1993) determined the frequency distributions of the peak luminosity [P: erg s^{-1}], the energy [E: erg], and flare duration [T: s] and found that the measured distributions could be best fitted with a cellular automaton model that produced powerlaw slopes of $\alpha_P = 1.86$, $\alpha_E = 1.51$, and $\alpha_T = 1.88$. The fits of the distributions included an exponential rollover at the upper end, which ex-

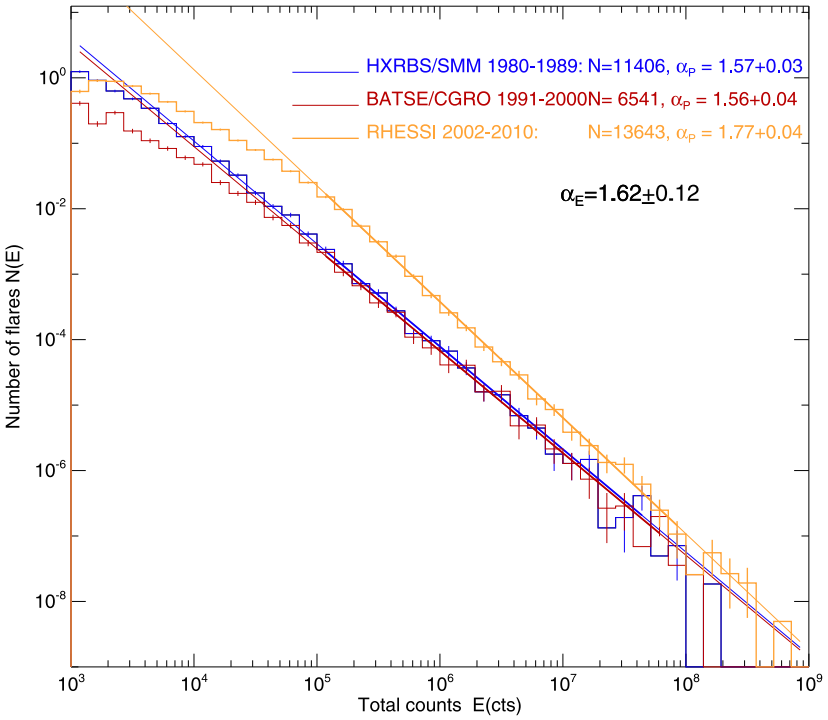

Figure 2 Occurrence frequency distributions of hard X-ray total counts or fluence [E: cts] observed with SMM/HXRBS (1980 – 1989), BATSE (1991 – 2000), and RHESSI (2002 – 2010), with powerlaw fits. An average preflare background of 40 cts s^{-1} multiplied with the flare duration was subtracted in the total counts of HXRBS.

plains why they inferred a less-steep slope for durations than previously reported. Lee, Petrosian, and McTiernan (1993) analyzed the same data and determined the correlations and frequency-distribution powerlaw slopes with special care of truncation biases and obtained similar values for ISEE-3 ($\alpha_P = 1.75$, $\alpha_E = 1.62$, $\alpha_T = 2.73$) as Crosby, Aschwanden, and Dennis (1993) for HXRBS. A third study was done with the same data (Bromund, McTiernan, and Kane, 1995), where the energy spectrum was also calculated to determine different energy parameters, similar to the study of Crosby, Aschwanden, and Dennis (1993), finding the following powerlaw slopes: $\alpha_P = 1.86, \ldots, 2.00$ for the peak photon flux [$P_{\rm ph}$: photons cm^{-2} s^{-1}], $\alpha_P = 1.92, \ldots, 2.07$ for the peak electron power [$P_{\rm e}$: erg s^{-1}], $\alpha_E = 1.67, \ldots, 1.74$ for the total electron energy [$E_{\rm e}$: erg], and $\alpha_T = 2.40, \ldots, 2.94$ for the total duration [T: s], where the range of powerlaw slopes results from the choice of the fitting range. The flare duration [T] was defined at a level of 1/e times the peak count rate.

From the latest solar mission with hard X-ray capabilities, the *Ramaty High-Energy Solar Spectroscopic Imager* (RHESSI) spacecraft, frequency distributions were determined in the 12 – 25 keV energy band from 2002 – 2005 (Su, Gan, and Li, 2006), finding powerlaw slopes of $\alpha_P = 1.80 \pm 0.02$ for the peak fluxes, and a broken powerlaw $\alpha_T = 0.9 - 3.6$ for the flare duration, similar to previous findings (see, *e.g.*, Crosby *et al.*, 1998). Christe *et al.* (2008) conducted a search for microflares and identified a total of $\approx 25\,000$ events observed with RHESSI during 2002 – 2007 and investigated the frequency distributions at lower energies, finding powerlaw slopes of $\alpha_P = 1.50 \pm 0.03$ for 3 – 6 keV peak count rates [$P_{\rm cts}$: cts s^{-1}],

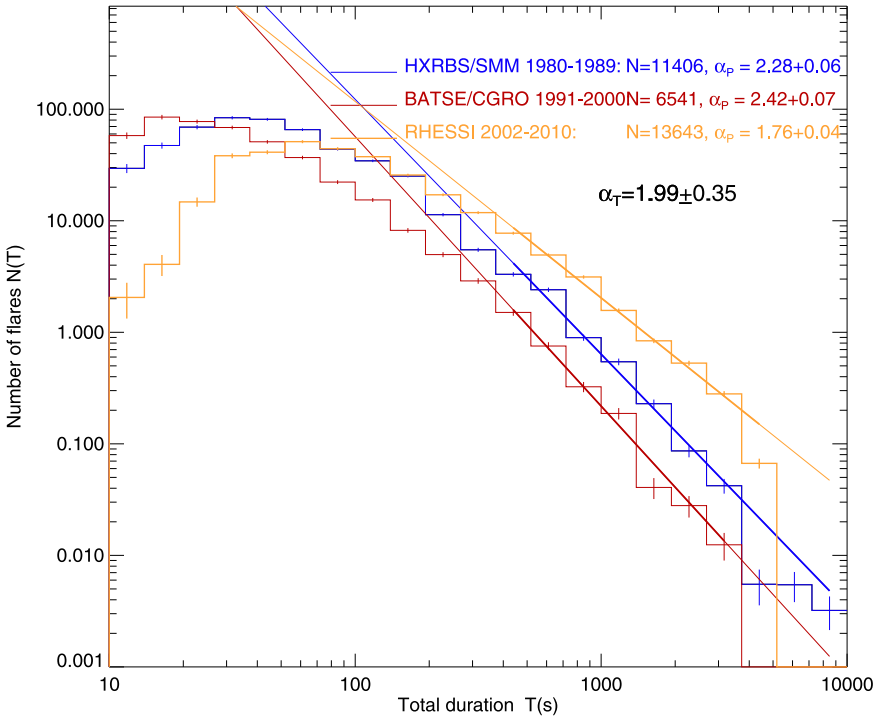

Figure 3 Occurrence-frequency distributions of hard X-ray flare durations [T: s] observed with SMM/HXRBS (1980 – 1989), BATSE (1991 – 2000), and RHESSI (2002 – 2010) with powerlaw fits. The flare durations for RHESSI were estimated from the time difference between the start and peak time, because RHESSI flare durations were determined at a lower energy of 12 keV (compared with 25 keV for HXRBS and BATSE), where thermal emission prolongs the nonthermal flare duration.

$\alpha_P = 1.51 \pm 0.03$ for 6 – 12 keV peak count rates, and $\alpha_P = 1.58 \pm 0.02$ for 12 – 25 keV peak count rates. Converting the peak count rates [P] into total energy fluxes by integrating their energy spectra, Christe *et al.* (2008) find an energy distribution with a powerlaw slope of $\alpha_E = 1.7 \pm 0.1$, with an average energy-deposition rate of $\lesssim 10^{26}$ erg s^{-1}. It is interesting that these microflare statistics are fairly consistent with overall flare statistics, even though it represents only a subset in the lowest energy range.

Flare statistics were also gathered from the *Solar X-ray/Cosmic Gamma-Ray Burst Experiment* (GRB) onboard the *Ulysses* spacecraft (Tranquille, Hurley, and Hudson, 2009), finding similar results for > 25 keV events, *i.e.* a powerlaw slope of $\alpha_P = 1.60 \pm 0.04$, which steepens to $\alpha_P = 1.75 \pm 0.08$ if the largest events with pulse pile-up are excluded.

We re-compiled statistics from existing flare catalogs from the three instruments SMM/HXRBS (1980 – 1989), CGRO/BATSE (1991 – 2000), and RHESSI (2002 – 2010) and show summary plots of the resulting frequency distributions in Figures 1 – 3. The powerlaw slopes are obtained from weighted linear regression fits, using the Poisson statistics of the number of events in each logarithmic bin (see Section 3.5). The average powerlaw slope for peak fluxes [$P_{\rm cts}$] is $\alpha_P = 1.73 \pm 0.07$ (Figure 1). The corresponding frequency distributions of total counts or fluences are shown in Figure 2, which have an average powerlaw slope of $\alpha_E = 1.62 \pm 0.12$ in the range of $E \geq 10^5$ cts. The distributions of flare durations are shown in Figure 3, which exhibit an average of $\alpha_T = 1.99 \pm 0.35$, with a tendency of a

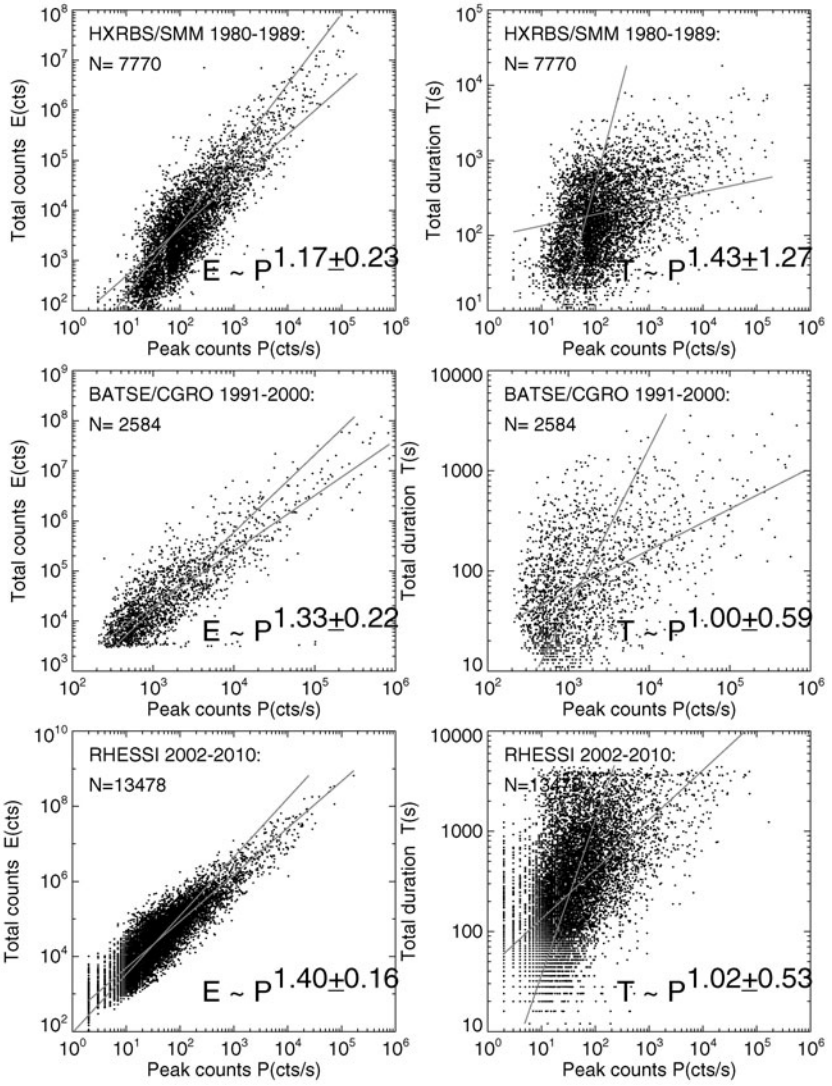

Figure 4 Scatterplots between the total counts $E(P)$ (left panels) or flare duration $T(P)$ (right panels) *versus* the peak count rate $[P_{\rm cts}]$ for solar flares with SMM/HXRBS (1980 – 1989) (top), CGRO/BATSE (1991 – 2000) (middle), and RHESSI (2002 – 2010) (bottom). Linear regression fits are applied for $y(x)$ and $x(y)$ (gray lines) and the listed values correspond to the average of the two linear regression fits.

rollover at the low end. Thus, our synthesized reference values are

$$\begin{aligned} N(P) &\propto P^{-\alpha_P}, \qquad \alpha_P = 1.73 \pm 0.07, \\ N(E) &\propto E^{-\alpha_E}, \qquad \alpha_E = 1.62 \pm 0.12, \\ N(T) &\propto T^{-\alpha_T}, \qquad \alpha_T = 1.99 \pm 0.35, \end{aligned} \tag{1}$$

which are compatible with most of the published values listed in Table 1. Thus, we can consider these synthesized values as representative means, averaged from three major missions over the last 30 years and three solar cycles, which can serve as a reference for the overall flare productivity of the Sun in hard X-ray wavelengths.

In Figure 4 we show the correlation plots between the parameters (sampled in Figures 1 – 3) and determine linear regression fits, which yield scaling laws of $E \propto P^{1.30\pm0.12}$ and $T \propto P^{1.15\pm0.24}$. Theoretically, these correlation coefficients can also be calculated from the powerlaw slopes of the frequency distributions. If two parameters x and y have powerlaw distributions $N(x) \propto x^{-\alpha_x}$ and $N(y) \propto y^{-\alpha_y}$, and the parameters are correlated by a powerlaw relationship $y \propto x^{\gamma}$, the powerlaw indices are related by $\gamma = (\alpha_x - 1)/(\alpha_y - 1)$ (see, *e.g.*, Aschwanden, 2010; Section 7.1.6). Therefore, based on the powerlaw slopes α_P, α_E, and α_T measured in Figures 1 – 3, we expect the following correlations between these three parameters:

$$\begin{array}{ll} E \propto P^{\gamma_E}, & \gamma_E = (\alpha_P - 1)/(\alpha_E - 1) = (1.73 - 1)/(1.62 - 1) = 1.2 \pm 0.2, \\ T \propto P^{\gamma_T}, & \gamma_T = (\alpha_P - 1)/(\alpha_T - 1) = (1.73 - 1)/(1.99 - 1) = 0.7 \pm 0.2. \end{array} \quad (2)$$

The correlation plots shown in Figure 4, where the linear regression fit is performed for $y(x)$ with x as independent variable, as well as for $x(y)$ with y as independent variable, respectively. The averaged powerlaw slopes (of both linear regression fits and all three datasets) yield values of $E \propto P^{1.3\pm0.2}$ and $T \propto P^{1.3\pm0.8}$, which are consistent with the values derived from the powerlaw slopes of the frequency distributions (Equation (2)), *i.e.* $E \propto P^{1.2\pm0.2}$ and $T \propto P^{0.7\pm0.2}$.

3. Uncertainties and Errors of Powerlaw Slopes

The determination of powerlaw slopes and their uncertainties is subject to methodological and data-selection effects. Given the variation of observed powerlaw slopes as listed in Table 1, it might be useful to briefly discuss some important selection effects and statistical uncertainties.

3.1. Energy or Wavelength Bias

In Table 1 we compare mostly flare data in the hard X-ray regime with energies of > 20 keV or > 25 keV, which all have similar powerlaw slopes of $\alpha_P \approx 1.6 - 1.8$. Even flares detected at lower energies > 8 keV (Lin, Feffer, and Schwartz, 2001) or > 12 keV (Su, Gan, and Li, 2006; Christe *et al.*, 2008) have similar powerlaw slopes. Also at the upper end, flares detected at high energies of > 100 keV (Perez Enriquez and Miroshnichenko, 1999) have similar powerlaw slopes. However, the same subset of flares observed at 0.075 – 124 MeV, from bremsstrahlung at 300 – 850 keV, from the 511 keV annihilation line fluence, from the 2.223 MeV neutron-line fluence, and from the 1 – 10 MeV γ-ray line fluence, have significantly flatter powerlaw slopes ($\alpha_P \approx 1.3 - 1.4$). This can be explained by the flatter energy spectra of large flares, which causes relatively higher fluxes at higher energies, and thus flatter occurrence-frequency distributions. Dennis (1985) has shown a systematic tendency of the hard X-ray spectrum as a function of the hard X-ray count rate, being generally flatter for large flares with high count rates, which predicts also flatter powerlaw slopes of the occurrence-frequency distributions at higher energies. Similar wavelength-bias effects occur also for flare fluxes detected in soft X-rays and EUV wavelengths, compared with hard

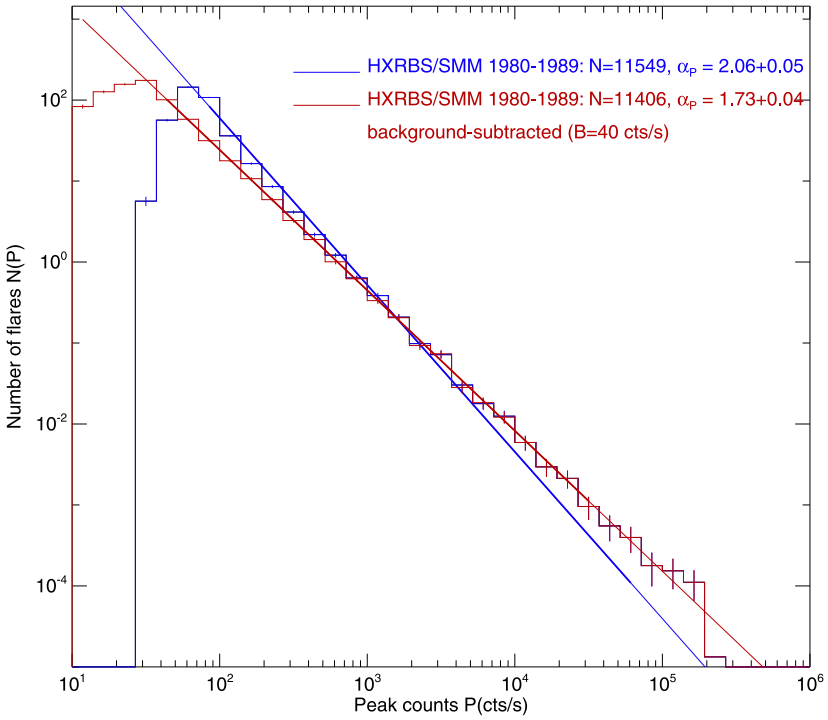

Figure 5 Occurrence-frequency distributions of hard X-ray peak count rates [$P_{\rm cts}$: cts s^{-1}] observed with SMM/HXRBS (1980 – 1989), without background subtraction ($\alpha_P = 2.06 \pm 0.05$; blue), and with subtraction of an average background of $B = 40$ cts s^{-1} ($\alpha_P = 1.73 \pm 0.01$; red).

X-ray fluxes, which depend on the physical emission mechanism. Therefore we confine our comparisons in Table 1 only to hard X-ray energies in the range of > 8 keV to > 100 keV here.

3.2. Effects of Data Gaps and Spacecraft Orbits

Data gaps due to spacecraft night or South Atlantic Anomaly (SAA) passages can also cause systematic biases, because they tend to shorten flare durations (due to interruption) and underestimate the total flare counts (due to incomplete sampling). These effects can in principle be simulated and their systematic effects on frequency distributions can be quantified this way. Numerical simulations of such selection and instrumental effects are also discussed in the context of waiting-time distributions (see, *e.g.*, Aschwanden and McTiernan, 2010). The distribution of peak fluxes is less affected by data gaps, as long as the peak of a flare is observed. Visual screening of flare light curves was carried out for events detected with SMM/HXRBS, so that missed flare peaks could be identified in the flare catalog (B.R. Dennis, private communication, 2010). For RHESSI flare catalogs, however, no correction for spacecraft-night datagaps has been applied to flare peak fluxes and fluences so far, and long-duration flares are counted multiple times for each spacecraft orbit (J.M. McTiernan, private communication, 2010).

3.3. Pre-event Background Subtraction

Most flare catalogs list the peak counts of flares without preflare-background subtraction, which has little impact on large flares, but leads to a strong overestimate of fluxes for the smallest flares, and thus systematically overestimates the powerlaw slope. We demonstrate this for the dataset of SMM/HXRBS flares. Figure 5 shows two (weighted) powerlaw fits, a steeper slope of $\alpha_P = 2.06 \pm 0.05$ for the uncorrected flare peak counts, and a flatter slope of $\alpha_P = 1.73 \pm 0.04$ after subtraction of an estimated average background of 40 cts s^{-1}. This correction was also applied in the original analysis by Crosby, Aschwanden, and Dennis (1993), and we use it here too. Note that the background-uncorrected distribution shows also a steepening of the powerlaw slope at the lower end.

For the RHESSI flare catalog, the preflare background is estimated to be $\approx 10-20$ cts s^{-1} per detector, the low limit applying to low spacecraft latitude, the high limit for high latitudes, with a mean of ≈ 12 cts s^{-1} per detector (J.M. McTiernan, private communication, 2010).

The subtraction of an average preflare background value is only a first-order correction, which may even cause events with negative peak fluxes when the background is time-varying. The optimum method would be to measure the preflare background for each event separately and to subtract it from the peak fluxes, as well as from the fluences before time integration.

3.4. Instrument Sensitivity

The instrumental sensitivity usually translates into a fixed flux threshold, which causes a sharp lower cutoff for peak flux distributions (Figures 1 and 5), but a gradual rollover for total fluence and duration of events (Figures 2 and 3). The rollover limits the scale-free range of the distribution over which a powerlaw can be fitted, and moreover produces a systematic bias for flatter powerlaw slopes when part of the rollover is included in the powerlaw fit. If powerlaw fits are weighted by the number of events per bin in a linear regression fit to a histogram, the lowest bins will have the highest weight, and thus a gradual rollover at the lower end will produce a too-flat powerlaw slope, when compared with the fit in the upper bins of the distribution. We determine the lower bound of the powerlaw fit range by the χ^2-criterion, which reliably detects a rollover by an excessive deviation from a powerlaw fit in terms of the expected standard deviation.

3.5. Linear Regression Fit Methods

A common method to determine powerlaw slopes is a linear regression fit to a histogram in a $\log(N)$–$\log(S)$ diagram, which can be done in two ways. If the frequency distribution closely follows a powerlaw function, a weighted linear regression fit can be performed in x log–y log space $\log(N)$ *vs.* $\log(S)$, or in x log–y lin space N *vs.* $\log(S)$, using the number of events per bin as relative weights. However, if the frequency distribution exhibits significant deviations from a straight powerlaw (*e.g.*, Figures 2 and 3), a weighted powerlaw fit can only be performed in a powerlaw-like subinterval. Often an unweighted fit (with equal weight in every bin) is carried out to obtain an approximate powerlaw slope. For the results given in the literature (as compiled in Table 1), it is not always clear whether the authors performed a weighted or unweighted linear regression fit, which may significantly deviate from each other depending on the fitted interval. In present study, we perform only weighted fits in well-defined intervals as described below.

In a x log–y log (or x log–y lin) histogram, the bins Δx_i on the x-axis are chosen to be of equal width on a log scale, corresponding to an exponentially increasing width on a linear scale. If $N(x)$ is the fitted function, the number of events N_i per bin depends on the variable (logarithmic) bin width Δx_i,

$$N_i = \int_{x_i}^{x_i+\Delta x_i} N(x)\,\mathrm{d}x \approx N(x_i)\Delta x_i. \tag{3}$$

The statistical uncertainty $[\sigma_i]$ in bin Δx_i due to Poissonian statistics is, in the Gaussian limit,

$$\sigma_i = \sqrt{N_i^{\mathrm{fit}}}, \tag{4}$$

and the statistical weighting factor $[w_i]$ for a linear regression fit that minimizes the squared standard deviations $[\sigma_i]$ is then,

$$w_i = \frac{1}{\sigma_i^2}. \tag{5}$$

The linear regression fit in x log–y lin space (in order to avoid asymmetric positive and negative uncertainties that result for x log–y log fits) finds then the following best-fit powerlaw function

$$N_i^{\mathrm{fit}} = N_0 (x_i)^{-\alpha}. \tag{6}$$

A criterion for the goodness of a fit is the χ^2-test, expressed with the so-called *reduced* χ^2-*value*, which expresses the mean deviation of the data points from the fitted function in units of expected standard deviations,

$$\chi_{\mathrm{red}} = \left[\frac{1}{(n - n_{\mathrm{free}})} \sum_{i=1}^{n} \frac{(N_i - N_i^{\mathrm{fit}})^2}{(\sigma_i)^2} \right]^{1/2}, \tag{7}$$

where n is the number of datapoints (or histogram bins here) and n_{free} is the number of free parameters of the fitted function, which is $n_{\mathrm{free}} = 2$ for a linear regression fit (with free parameters N_0 and α in Equation (6)). However, while bins with a large number of events ($\gtrsim 10$) are well approximated by a Gaussian, with an uncertainty of $\sigma_i = \sqrt{N_i^{\mathrm{fit}}}$ about the expectation value N_i^{fit}, the Poisson probability distribution deviates significantly from a Gaussian for bins with fewer events. For this case, the χ^2-test has to be replaced with C-statistics (Cash, 1979), which has the following expression corresponding to the reduced χ^2-criterion

$$\chi_{\mathrm{Cash}} = \left[\frac{2}{(n - n_{\mathrm{free}})} \sum_{i=1}^{n} N_i \ln\left(N_i / N_i^{\mathrm{fit}}\right) - \left(N_i - N_i^{\mathrm{fit}}\right) \right]^{1/2}, \tag{8}$$

where N_i^{fit} is the theoretical expectation value based on the best-fit powerlaw function and has to be positive for all fitted bins. For an acceptable powerlaw fit, approximately a value of $\chi_{\mathrm{Cash}} \approx 1.0$ is expected. However, the distribution of the C-statistic values is not always peaked at 1.0 as the χ^2 probability distribution is, but instead depends on the expectation values of the number of counts per bin, when the majority of bins have a low number of events (Nousek and Shue, 1989; Schmahl, 1999a, 1999b). The linear regression fit then yields a powerlaw slope α and a probable uncertainty σ_α derived from minimizing either the χ^2 or the C-statistics.

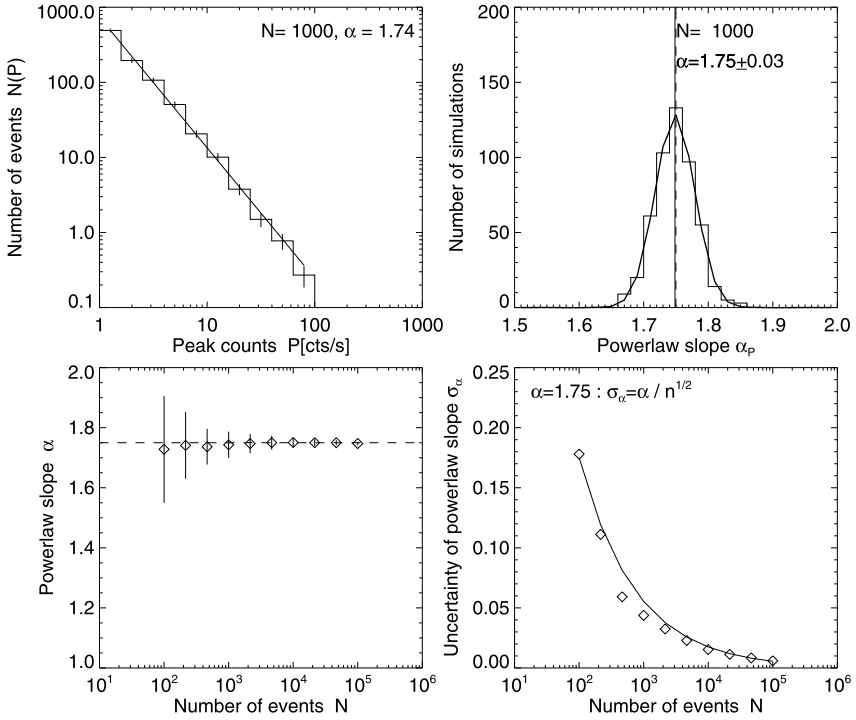

Figure 6 Monte-Carlo simulations of powerlaw distributions carried out for a theoretical powerlaw slope of $\alpha = 1.75$ with different random representations according to Equation (11). A single distribution based on $N = 1000$ events is shown with powerlaw fit $\alpha = 1.74$ (top left panel). The Gaussian distribution of powerlaw slopes obtained from $N_{\rm run} = 1000$ runs with different random representations yields a mean of $\alpha = 1.75 \pm 0.03$ (top right). These Monte-Carlo simulations are repeated for various number of events $N = 10^2, \ldots, 10^5$, which show a convergence of the mean value and standard deviations toward the theoretical value $\alpha = 1.75$ (bottom left). The scaling of the standard deviation $\sigma_\alpha(N) = \alpha/\sqrt{N}$ as a function of the number of events N is also shown (bottom right).

3.6. Monte-Carlo Simulations of Powerlaw Uncertainty

We verify these results with a Monte-Carlo simulation. Mathematically, a desired distribution function $f(x)$ can be generated from uniformly distributed random values ρ in the range of [0, 1] by using the inverse function $F^{-1}(x)$ of the integral function $F(x)$ of $f(x)$. Here we wish to generate a frequency distribution of energies E in the form of a powerlaw function $p(E)$ with slope α (Aschwanden, 2010, Section 7.1.5),

$$p(E) = (\alpha - 1)E^{-\alpha}, \tag{9}$$

which fulfills the normalization $\int_1^\infty p(E)\,{\rm d}E = 1$. The total probability $\rho(E)$ in the range $[0, E]$ is then the integral function of $p(E)$ (Equation (9)),

$$\rho(E) = \int_0^E p(\epsilon)\,{\rm d}\epsilon = \int_0^E (\alpha - 1)\epsilon^{-\alpha}\,{\rm d}\epsilon = \left[1 - E^{(1-\alpha)}\right]. \tag{10}$$

The inverse function $E(\rho)$ of $\rho(E)$ (Equation (10)) is

$$E(\rho) = [1 - \rho]^{1/(1-\alpha)}. \tag{11}$$

In Figure 6 (top left) we use a random generator that produces 1000 values $[\rho_i]$ uniformly distributed in the range of [0, 1], choose a powerlaw index of $\alpha = 1.75$, and use the transform Equation (11) to generate values $E_i = [1 - \rho_i]^{1/(1-\alpha)}$ and sample the frequency distribution of the 1000 values E_i, which produces a powerlaw function $p(E) = (\alpha - 1)E^{-\alpha}$ as defined in Equation (9), with a best-fit slope of $\alpha = 1.74$.

We repeat the generation of powerlaw histograms with $N = 1000$ different random representations ρ_i and find for the powerlaw slopes a Gaussian distribution with a mean and standard deviation of $\alpha = 1.75 \pm 0.03$ (Figure 6, top right). The spread of α-values is expected to depend on the number N of events in the distribution. In order to quantify this dependence we repeat the same exercise for different numbers of events in the range of $N = 10^2, \ldots, 10^5$, which is shown in Figure 6 (bottom left). The standard deviations σ_α of the powerlaw slope distributions is found to depend on the number of events (per distribution) as

$$\sigma_\alpha(N) = \frac{\alpha}{\sqrt{N}}, \tag{12}$$

as expected for a normal distribution of random values generated by a large number of Monte-Carlo simulations. Equation (12) can be used to estimate the accuracy of the powerlaw slope from the number of events. For instance, for a dataset of $N = 10^4$ events, an accuracy of $\sqrt{N} = 1\%$ is expected for the value of the powerlaw slope.

4. Solar-Flare Statistics *versus* Solar Cycle

We investigate now whether the statistical distributions of the most reliably determined flare parameter, namely the peak flux P, exhibits significant changes during the solar cycle. The approximately sinusoidal variation of the flare rate during the last three Solar Cycles 21, 22, and 23 is shown in Figure 7, where we have SMM/HXRBS coverage during 1980 – 1989 (Cycle 21 and part of 22), CGRO/BATSE coverage during 1991 – 2000 (end of Cycle 22 and start of Cycle 23), and RHESSI coverage during 2002 – 2010 (Cycle 23). After eliminating questionable events from the flare catalog (*i.e.*, events with energy gain changes, time discrepancies, missing peak flux, negative peak flux after background subtraction, or pile-up events), we are left with 9374 flare events observed with SMM/HXRBS, 6542 flare events observed with CGRO/BATSE, and 12 147 flare events with RHESSI. The list of peak fluxes obtained from the currently existing flare catalogs has to be taken with a grain of salt, because the peak flux was missed in some flare events in spacecraft-orbit night, or some long-duration events were counted multiple times when they overlapped multiple spacecraft orbits (in particular for RHESSI), or the preflare flux was subtracted with an average constant, while it is time-variable in reality. The effect of the background subtraction on the slope of the powerlaw distribution of peak fluxes is shown in Figure 5, but the effect of the other shortcomings on the powerlaw slope is not well-known and needs to be corrected on an event-by-event basis, using auxiliary data such as GOES light curves.

In order to eliminate any bias of powerlaw fits related to the number of events per subset (since the accuracy of the fitted powerlaw slope scales with $N^{-1/2}$, *i.e.* Equation (12)), we subdivide the dataset of each instrument into subsets with equal event numbers, of the order of 2000 events per subset. This way we obtain 12 subsets, consisting of four HXRBS subsets

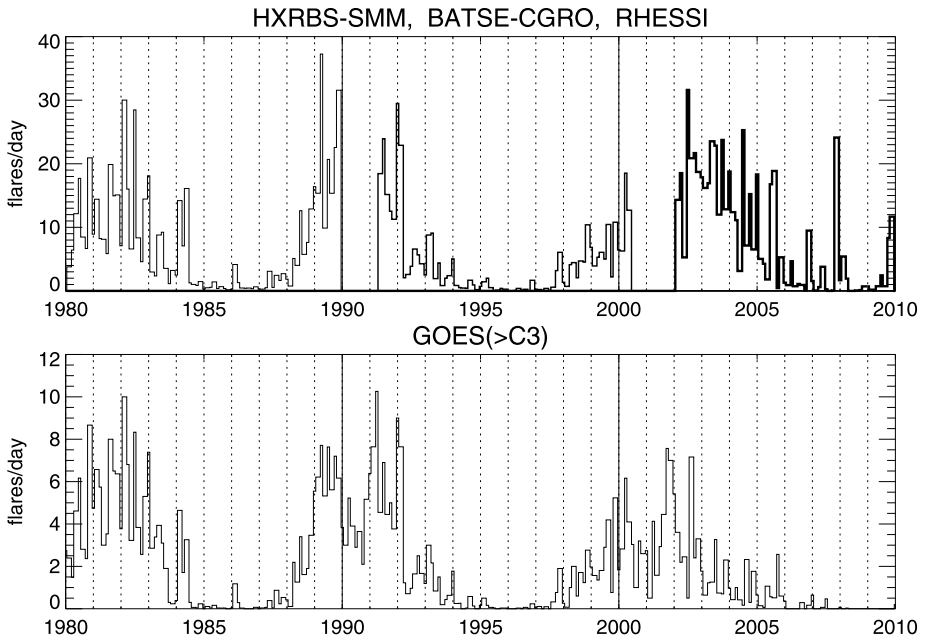

Figure 7 Top: Monthly averages of solar-flare rates observed during the last three solar cycles in hard X-rays with SMM/HXRBS (1980 – 1989), CGRO/BATSE (1991 – 2000), and RHESSI (2002 – 2010). Bottom: Monthly averages of solar-flare rate observed in soft X-rays with GOES, including events above the C3-class level.

(with 2343 events each), three BATSE subsets (with 2180 events each), and five RHESSI subsets (with 2429 events each). The time ranges of these 12 equal-sized data subsets are listed in Table 2, and the corresponding frequency distributions with the powerlaw fits are shown in Figure 8, along with the slopes [α_P] and χ^2-tests in terms of Cash statistics ($\chi_{\rm Cash}$). The fitted ranges of peak fluxes [P_1, P_2] are chosen to start at the next bin above the maximum of the frequency distribution, and to span four orders of magnitude, with a logarithmic binning of seven bins per decade.

In order to investigate the temporal dependence of the powerlaw slopes of peak-flux distributions, we plot the values $\alpha_P \pm \sigma_\alpha$ in the second panel of Figure 9, where all subsets have the same uncertainty in the powerlaw slope, but cover time intervals of variable lengths, *i.e.* smaller time intervals during solar maxima and longer time intervals during solar minima, because of our requirement of equal number statistics in each subset. For comparison, we also plot the published values of datasets, which includes datasets 3 – 8, and 12 – 14 from Table 1 (Figure 9, top panel). The datasets labeled with 17 – 19 in the middle panel correspond to HXRBS, BATSE, and RHESSI as listed in Table 2 and analyzed in Figures 1 – 4 and 8. In the third panel of Figure 9 we repeat the same procedure with smaller data subsets of approximately 1000 events per subset, in order to have a higher temporal resolution of the cycle variation.

The temporal variation of the powerlaw slope $\alpha_P(t)$ as shown in Figure 9 appears to have a cyclic modulation that is anti-correlated with the solar cycles. Since three solar cycles contain three maxima and three minima, we fit a sixth-order polynomial to the data, as shown in the second and third panel in Figure 9. The powerlaw slopes reach relative maxima during the minima of the solar cycles, *i.e.* $\alpha_P = 1.79$ in $t \approx 1986$ (between Cycle 21 and 22),

Table 2 Frequency distributions measured from solar flares in hard X-rays during the solar cycle.

Instrument	Years	Number of events [n]	Lower fit bound [P_1]	Upper fit bound [P_2]	Powerlaw slope of peak counts [$\alpha_P \pm \sigma_\alpha$]	Goodness of fit [$\chi_{\rm Cash}$]
HXRBS	1980.1 – 1981.2	2343	43	43 939	1.79±0.02	0.74
HXRBS	1981.2 – 1982.1	2343	43	61 054	1.75±0.02	1.21
HXRBS	1982.1 – 1983.6	2343	43	117 876	1.73±0.02	0.88
HXRBS	1983.6 – 1989.0	2343	31	84 834	1.79±0.02	1.07
BATSE	1991.3 – 1992.0	2180	610	848 343	1.64±0.02	0.62
BATSE	1992.0 – 1995.0	2180	439	227 584	1.62±0.02	1.34
BATSE	1995.0 – 2000.0	2180	610	848 343	1.69±0.02	0.64
RHESSI	2002.1 – 2002.7	2429	16	16 378	1.68±0.02	1.19
RHESSI	2002.7 – 2003.4	2429	16	11 787	1.71±0.02	1.82
RHESSI	2003.4 – 2004.2	2429	16	61 054	1.66±0.02	1.61
RHESSI	2004.2 – 2005.4	2429	16	84 834	1.69±0.02	1.20
RHESSI	2005.4 – 2010.0	2429	22	16 378	1.76±0.02	1.88

$\alpha_P \approx 1.69$ in $t \approx 1999$ (between Cycle 22 and 23), and $\alpha_P \approx 1.76$ in $t \approx 2008$, the recent extended solar minimum. During the solar maxima or one – two years later, the powerlaw slopes reach their minimum values, so the frequency distributions are flattest then. We show the cycle variation of GOES >C3-class flares in the bottom panel of Figure 9.

This is a novel result that could be interpreted as a solar-cycle dependence of the powerlaw slope of flare hard X-ray count rate distributions. The variation of the powerlaw slope is anti-correlated with the flare rate or sunspot number, being steepest during solar minima and flattest during solar maxima. The absolute values of the powerlaw slope do not cover the same range in each solar cycle, but it is not clear whether this reflects a property of strong and weak cycles, or could be an artifact of the different instruments and the individual flare-detection algorithms, since we used a different instrument for each solar cycle. Therefore, some of the variation could be due to a systematic difference between the three different instruments used in each cycle, especially since the absolute values and the relative change between solar maxima and minima is different for each instrument. In particular for the RHESSI data set, it is suspected that significant radiation damage before annealing in 2007 and 2010 could distort the flare statistics, which may also be indicated by the deviation from a good powerlaw fit (with a $\chi_{\rm Cash} = 1.878$ for the time interval of 2005.4 – 2010.0 in Figure 8, bottom right). Moreover, the RHESSI flare catalog is biased by multiple counting of flares that overlap multiple orbits and by missed flare peaks in the spacecraft night of the orbit. However, despite these instrumental effects, the powerlaw slope appears to be systematically steeper during the solar minima compared with the preceding solar maximum for each cycle and instrument (Figure 9, second and third panel).

5. Discussion and Conclusions

Frequency distributions of solar-flare parameters have been reported over the last three solar cycles from different instruments and different phases of the solar cycle, covering a scattered

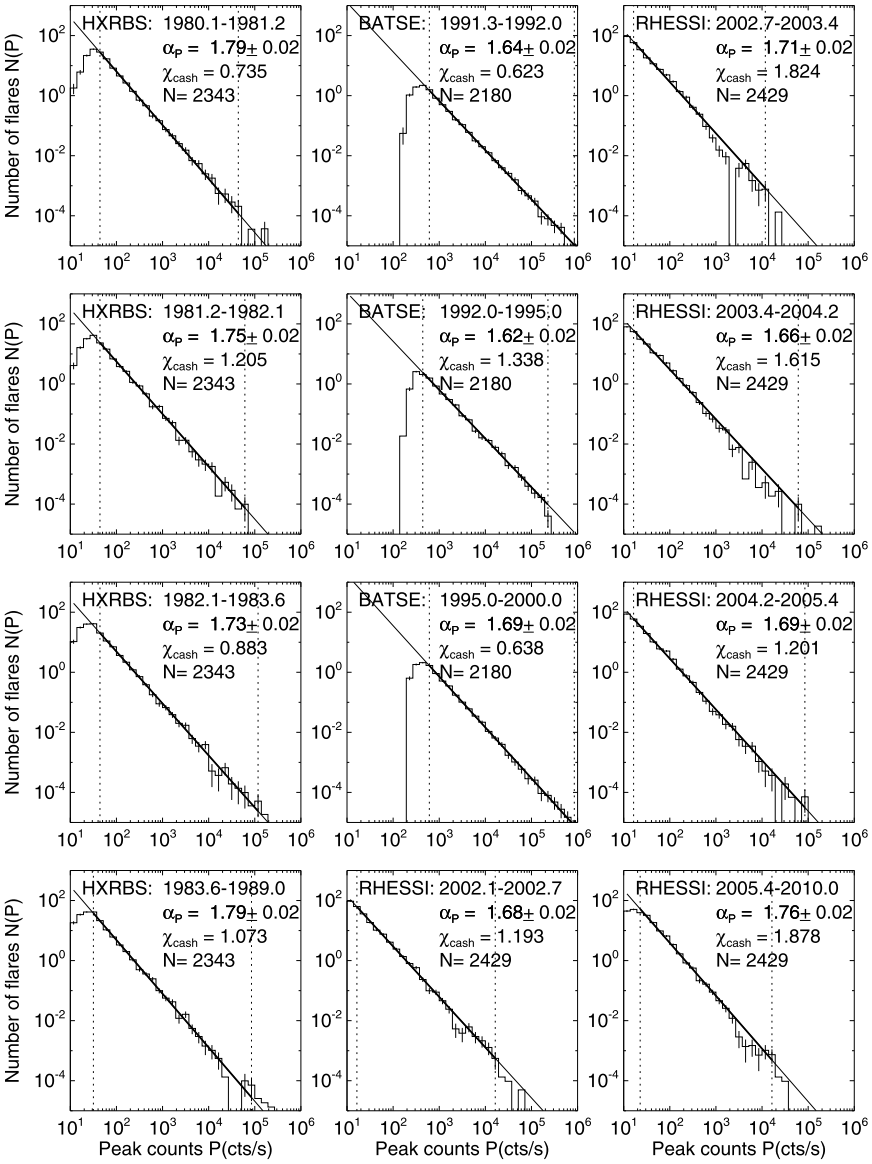

Figure 8 Occurrence-frequency distributions of hard X-ray peak count rates [$P_{\rm cts}$: cts s^{-1}] observed with SMM/HXRBS, CGRO/BATSE, and RHESSI, broken down into 12 time intervals with equal number of events in each subset. The powerlaw fits were determined with weighted powerlaw fits within a range [P_1, P_2] marked with dotted vertical lines. The best-fit powerlaw function is marked with thick solid linestyle and the values and uncertainties are also listed in Table 2 and plotted as a function of time in Figure 9.

range of values (Table 1). Powerlaw slopes were reported in a range of $\alpha_P \approx 1.6-2.0$ for peak fluxes (counts), $\alpha_E \approx 1.4-1.7$ for total fluxes (fluences), and $\alpha_T \approx 1.9-2.8$ for total durations, if we restrict to the hard X-ray range of $\approx 10-100$ keV. Averaging the powerlaw slopes from the largest datasets spanning entire solar cycles (using data from SMM/HXRBS,

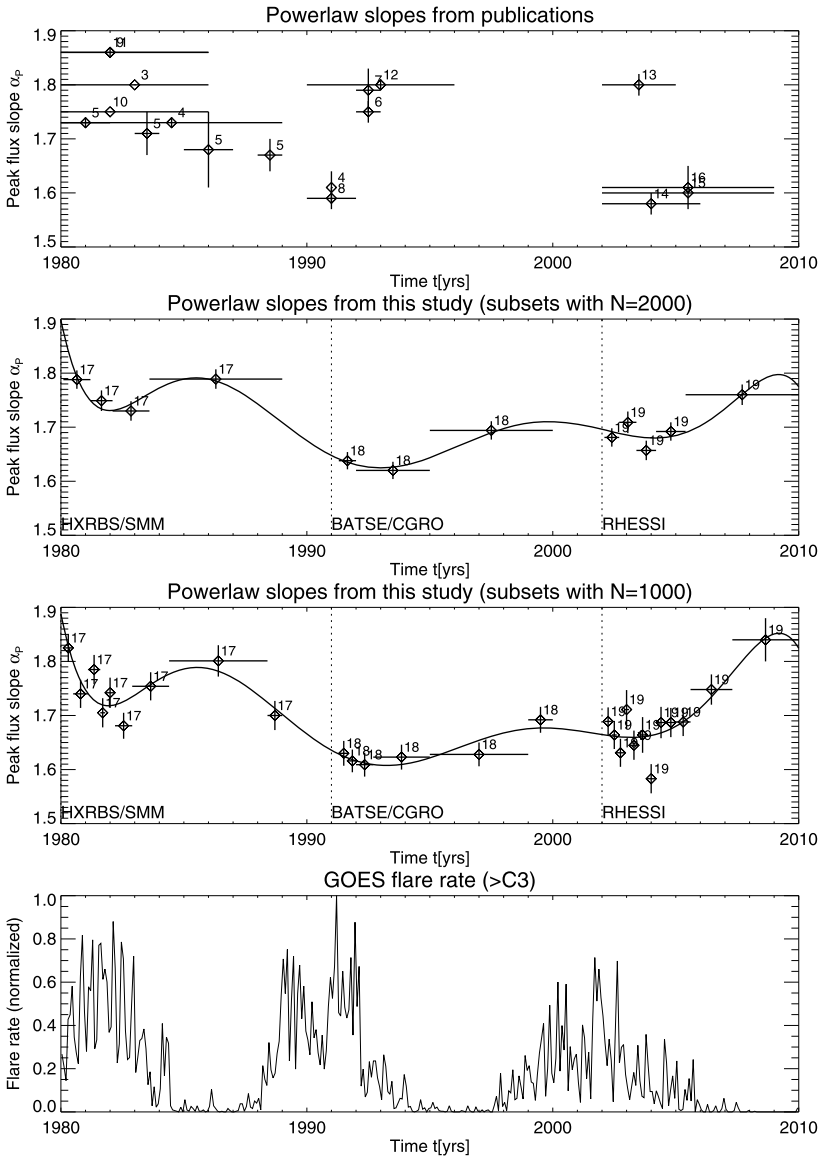

Figure 9 The powerlaw slope $[\alpha_P]$ of the peak flux $[P]$ as a function of time during the last three solar cycles is shown for values quoted in the literature (top panel), for HXRBS, BATSE, and RHESSI data analyzed in our study with equal-sized subsets of ≈ 2000 events per subset (second panel) or ≈ 1000 events per subset (third panel), along with the flare rate observed by GOES (bottom panel). The diamond symbols and numbers indicate the mean values of α_P and the corresponding reference number quoted in Table 1. The horizontal bars indicate the time intervals of the data subsets and the vertical bars indicate the uncertainties. The functional dependence of the powerlaw slope $[\alpha_P(t)]$ on the solar cycle is fitted with a sixth-order polynomial.

CGRO/BATSE, RHESSI), we find mean values of $\alpha_P = 1.73 \pm 0.07$ for peak fluxes (Figure 1), $\alpha_E = 1.62 \pm 0.12$ for fluences (Figure 2), and $\alpha_T = 1.99 \pm 0.35$ for flare durations (Figure 3). Investigating variations of the flare statistics as a function of time, we find evi-

dence for a significant variation of the powerlaw slope of the frequency distributions during the solar cycle. We find that the powerlaw slope is systematically flatter during the solar cycle maxima compared with the following solar cycle minimum, for each of the three solar cycles and instrumental periods (on the order of $\Delta\alpha \approx 0.1$), in anti-correlation with the sunspot number.

Why is our result of the anti-correlation of the powerlaw slope of flare count rates with the solar cycle not evident from previously published values? First of all, the datasets have been subject to inconsistent analysis methods by different authors, differing in the type of linear regression fits (weighted *versus* unweighted), the fitted range $[P_1, P_2]$, selection effects of events (flare catalogs *versus* automated microflare search algorithms), background treatment (with or without background subtraction), as discussed in Section 3. Part of the solar-cycle variation could be due to instrumental effects, especially since the absolute values of the powerlaw slopes vary by different amounts between solar-cycle maxima and minima for the three instrumental periods. It is also suspected (B.R. Dennis, private communication, 2011) that the generally higher values obtained from HXRBS data before 1989 and from RHESSI after 2006 are not real but rather reflect a difference between the instruments, and the pre- and post-anneal phases of RHESSI observations. Nevertheless, despite the uncertainties of the absolute values, there seems to be a tendency of flatter powerlaw slopes during the solar maxima, compared with the following solar-cycle minimum. The fact that the Sun produces flatter occurrence-frequency powerlaw slopes during periods of high flare activity indicates that hard X-ray spectra are systematically flatter, so that more nonthermal energy is contained in a bremsstrahlung spectrum, for the same amount of detected photons above an energy of $E > 25$ keV. This is not unexpected, since a correlation between the hard X-ray flux and the spectral slope was already noticed early on (Dennis, 1985).

Marginal variations of the powerlaw slope with flare activity have been noted before. Crosby, Aschwanden, and Dennis (1993; Figure 12 therein) found variations of the powerlaw slope during the solar cycle in excess of the statistical uncertainties of the linear regression fits, but no clear functional dependence on the solar cycle was found. Biesecker (1994) noticed slight differences of the powerlaw slope during low-activity ($\alpha_P = 1.71 \pm 0.04$) and high-activity periods ($\alpha_P = 1.68 \pm 0.02$), with the powerlaw slope usually flatter for high-activity periods, which is analogous to our finding a flatter slope during solar-cycle maxima. Bai (1993) devised a special maximum-likelihood method to determine the powerlaw slope of flare distributions from SMM/HXRBS and found some variation of the powerlaw slope correlated with a 154-day periodicity of flare rates. He found that the size distributions are steeper during the maximum years of Solar Cycle 21 (1980 and 1981) than in the declining phase (1982 – 1984). Thus, the three studies (Bai, 1993; Biesecker, 1994; and this study) agree in the result that a flatter powerlaw slope is correlated with a higher flare activity, either on periods of recurrent flare activity (153.8 days) or solar cycles (12.6 years).

What does our novel result suggest for the physical interpretation? A flatter frequency distribution implies an over-proportional amount of larger events, compared with an averaged distribution. This means that the physical conditions vary during the solar cycle. One possible explanation could be that the magnetic complexity increases during solar maximum, which produces more stressing of magnetic fields and larger energy releases. The magnetic fields during the maximum of the solar cycle are dominated by the toroidal component of the solar dynamo, which entails higher magnetic stresses. The magnetic field during the minimum of the solar cycle is simpler and is dominated by the dipolar poloidal field that spans from the North to the South Pole. It appears that the relative amount of energy released in flares is modulated by the magnetic-field complexity of the solar dynamo. Theoretical models that reproduce the statistical distributions of solar flares in terms of the concept of self-organized criticality are discussed in Paper II (Aschwanden, 2011).

Acknowledgements We thank the referee Brian Dennis and James McTiernan for constructive and helpful comments that substantially improved this study. This work is partially supported by NASA contract NAS5-98033 of the RHESSI mission through the University of California, Berkeley (subcontract SA2241-26308PG) and NASA grant NNX08AJ18G. We acknowledge access to solar data and flare catalogs from the *Solar Data Analysis Center* (SDAC) at the NASA Goddard Space Flight Center (GSFC).

References

Aschwanden, M.J.: 2010, *Self-Organized Criticality in Astrophysics. The Statistics of Nonlinear Processes in the Universe*. Springer-Praxis, Heidelberg. ISBN:3642150004.

Aschwanden, M.J.: 2011, The state of self-organized criticality of the sun during the last three solar cycles. II. Theoretical modeling. *Solar Phys.*, accepted, Paper II.

Aschwanden, M.J., McTiernan, J.M.: 2010, Reconciliation of waiting time statistics of solar flares observed in hard X-rays. *Astrophys. J.* **717**, 683 – 692.

Bai, T.: 1993, Variability of the occurrence frequency of solar flares as a function of peak hard X-ray rate. *Astrophys. J.* **404**, 805 – 809.

Biesecker, D.A.: 1994, On the occurrence of solar flares observed with the Burst and Transient Source Experiment. Ph.D. Thesis, University of New Hampshire.

Biesecker, D.A., Ryan, J.M., Fishman, G.J.: 1994, Observations of small solar flares with BATSE. In: Ryan, J.M., Vestrand, W.T. (eds.) *High-Energy Solar Phenomena – A New Era of Spacecraft Measurements*, American Inst. Physics, New York, 183 – 186.

Biesecker, D.A., Ryan, J.M., Fishman, G.J.: 1993, A search for small solar flares with BATSE. In: *Lecture Notes in Physics* **432**, 225 – 230.

Bromund, K.R., McTiernan, J.M., Kane, S.R.: 1995, Statistical studies of ISEE3/ICE observations of impulsive hard X-ray solar flares. *Astrophys. J.* **455**, 733 – 745.

Cash, W.: 1979, Parameter estimation in astronomy through application of the likelihood ratio. *Astrophys. J.* **228**, 939 – 947.

Christe, S., Hannah, I.G., Krucker, S., McTiernan, J., Lin, R.P.: 2008, RHESSI microflare statistics. I. Flare-finding and frequency distributions. *Astrophys. J.* **677**, 1385 – 1394.

Crosby, N.B.: 1996, Contribution à l'Etude des Phénomènes Eruptifs du Soleil en Rayons à partir des Observations de l'Expérience WATCH sur le Satellite GRANAT. PhD Thesis, Université Paris VII, Meudon, Paris.

Crosby, N.B., Aschwanden, M.J., Dennis, B.R.: 1993, Frequency distributions and correlations of solar X-ray flare parameters. *Solar Phys.* **143**, 275 – 299.

Crosby, N.B., Vilmer, N., Lund, N., Sunyaev, R.: 1998, Deka-keV X-ray observations of solar bursts with WATCH/GRANAT: frequency distributions of burst parameters. *Astrophys. J.* **334**, 299 – 313.

Datlowe, D.W., Elcan, M.J., Hudson, H.S.: 1974, OSO-7 observations of solar X-rays in the energy range 10 – 100 keV. *Solar Phys.* **39**, 155 – 174.

Dennis, B.R.: 1985, Solar hard X-ray bursts. *Solar Phys.* **100**, 465 – 490.

Lee, T.T., Petrosian, V., McTiernan, J.M.: 1993, The distribution of flare parameters and implications for coronal heating. *Astrophys. J.* **412**, 401 – 409.

Lin, R.P., Feffer, P.T., Schwartz, R.A.: 2001, Solar hard X-ray bursts and electron acceleration down to 8 keV. *Astrophys. J.* **557**, L125 – L128.

Lin, R.P., Schwartz, R.A., Kane, S.R., Pelling, R.M., Hurley, K.C.: 1984, Solar hard X-ray microflares. *Astrophys. J.* **283**, 421 – 425.

Lu, E.T., Hamilton, R.J., McTiernan, J.M., Bromund, K.R.: 1993, Solar flares and avalanches in driven dissipative systems. *Astrophys. J.* **412**, 841 – 852.

Nousek, J.A., Shue, D.R.: 1989, *Astrophys. J.* **342**, 1207 – 1211.

Perez Enriquez, R., Miroshnichenko, L.I.: 1999, Frequency distributions of solar gamma ray events related and not related with SPEs 1989 – 1995. *Solar Phys.* **188**, 169 – 185.

Schmahl, E.: 1999a, http://hesperia.gsfc.nasa.gov/schmahl/c-statistic/node1.html.

Schmahl, E.: 1999b, http://hesperia.gsfc.nasa.gov/schmahl/cash/cash_oddities.html.

Schwartz, R.A., Dennis, B.R., Fishman, G.J., Meegan, C.A., Wilson, R.B., Paciesas, W.S.: 1992, BATSE flare observations in solar cycle 22. In: Shrader, C.R., Gehrels, N., Dennis, B.R. (eds.) *The Compton Observatory Science Workshop*, *NASA* **CP-3137**. NASA, Washington, 457.

Su, Y., Gan, W.Q., Li, Y.P.: 2006, A statistical study of RHESSI flares. *Solar Phys.* **238**, 61 – 72.

Tranquille, C., Hurley, K., Hudson, H.S.: 2009, The Ulysses catalog of solar hard X-ray flares. *Solar Phys.* **258**, 141 – 166.